

Feasibility Study on Disentangling Muscle Movements in TMR Patients Through a Myokinetic Control Interface for the Control of Artificial Hands

Marta Gherardini ¹, *Student Member, IEEE*, Agnes Sturma, Anna Boesendorfer, Valerio Ianniciello ²,
Andrea Mannini ³, Oskar C. Aszmann ⁴, and Christian Cipriani ⁵, *Senior Member, IEEE*

Abstract—Targeted muscle reinnervation (TMR) is a surgical procedure which allows to restore myoelectric control sources in people with proximal upper-limb amputations. However, the large physical displacement generally provoked by the reinnervated muscles following contraction can represent a drawback for the use of surface electrodes, which are affected by movement artifacts. In this regard, the viability of directly exploiting the physical displacement of muscles as control source would be beneficial. We recently introduced the so called *myokinetic interface*, aimed at transducing muscle movements into decipherable signals for artificial hands by tracking magnetic markers implanted inside the muscles. This work features the combination of the TMR procedure with such interface, in a non-invasive way. Two participants who underwent TMR surgery following above-the-elbow amputation were enrolled in this study. During two experimental sessions, we assessed the feasibility of: (i) disentangling muscle displacements associated with different degrees of freedom (DoFs) of the missing limb through video analysis, and (ii) discriminating different DoFs by tracking the displacement of five magnetic markers placed on the skin, over the reinnervated sites. A simple logistic regressor proved able to discriminate three different DoFs (six movements), with an average F1-score among classes and testing conditions of 0.84 (0.65) and 0.69 (0.60) for the video and the myokinetic data, for

the first (second) participant, respectively. The presented outcomes encourage further investigations, and pave the way towards novel control strategies for artificial hands in TMR patients.

Index Terms—Prosthetics and Exoskeletons, visual tracking, localization.

I. INTRODUCTION

IN ITALY and the U.K., approximately 3500 and 5200 new upper limb amputations are reported every year [1]. Arm amputations are mostly caused by traumatic events (industrial accidents, motor vehicle collisions, etc.), followed by vascular disease and cancer [2]. In other cases, limb amputations can be ascribed to congenital conditions, though they represent <1% the total incidence in the US [3]. No matter what the cause, the loss of a hand results in an important functional impairment, hindering the execution of simple tasks of daily living, both at home and at work. Important social aspects must also be considered: we do not use our hands only to grasp objects, but also to communicate with each other and to interact with the environment. Note, approximately 70% of amputees experience phantom limb pain [2]. For these reasons, several solutions have been investigated in the past to help patients regain upper extremity functions and release them from pain [2]. In the recent years the advances in technology and amputation surgery have led to important improvements in signal extraction and interpretation [4]–[6], prosthetic devices [7], [8], and suspension systems [9], [10].

As an example, the Targeted Muscle Reinnervation (TMR) surgical procedure proved beneficial both for the control efficiency [5] and the prevention and treatment of phantom limb pain [2]. It consists in redirecting nerves that would innervate the muscles of the missing limb to reinnervate surrogate muscles to be used as control sources, and proved to be very effective in patients with proximal amputations. Control signals are usually derived from the reinnervated muscles electrical activity, using the surface electromyogram (sEMG) [5] or Implantable Myoelectric Sensors (IMES) [4], [11]. The former presents several drawbacks, such as poor selectivity, skin-electrode adherence dependence and movement artifacts, to cite a few [2], [12]. The latter are directly inserted into the muscles, therefore their selectivity and signal to noise ratio are significantly improved. Nevertheless, IMES are active components which are implanted permanently inside the body, and need to be powered through wireless energy transfer across the body tissues.

Manuscript received February 24, 2022; accepted May 31, 2022. Date of publication June 10, 2022; date of current version June 20, 2022. This letter was recommended for publication by Associate Editor D. Oetomo and Editor P. Valdastris upon evaluation of the reviewers' comments. This work was supported in part by the European Research Council, through the MYKI Project under Grants ERC-2015-StG and 679820 and in part by the Natural BionicS Project, ERC Synergy Grant under Grant 810346. (*Corresponding author: Marta Gherardini.*)

Marta Gherardini, Valerio Ianniciello, and Christian Cipriani are with the Biorobotics Institute, Scuola Superiore Sant'Anna, 56025 Pontedera, PI, Italy, and also with the Department of Excellence in Robotics & AI, Scuola Superiore Sant'Anna, 56127 Pisa, Italy (e-mail: marta.gherardini@santannapisa.it; valerio.ianniciello@santannapisa.it; ch.cipriani@sssup.it).

Agnes Sturma, Anna Boesendorfer, and Oskar C. Aszmann are with the Clinical Laboratory for Bionic Extremity Reconstruction, Department of Plastic, Reconstructive and Aesthetic Surgery, Medical University of Vienna, 1090 Vienna, Austria (e-mail: agnes.sturma@meduniwien.ac.at; anna.boesendorfer@meduniwien.ac.at; oskar.aszmann@meduniwien.ac.at).

Andrea Mannini is with the IRCCS Fondazione Don Carlo Gnocchi Onlus, 50143 Firenze, Italy (e-mail: a.mannini@sssup.it).

This work involved human subjects or animals in its research. Approval of all ethical and experimental procedures and protocols was granted by Ethical Committee of the Medical University of Vienna (MUV) under Application No. EK Nr: 1393/2021, and performed in line with the Declaration of Helsinki.

This paper has supplementary downloadable material available at <http://ieeexplore.ieee.org>.

This letter has supplementary downloadable material available at <https://doi.org/10.1109/LRA.2022.3181748>, provided by the authors.

Digital Object Identifier 10.1109/LRA.2022.3181748

We recently proposed in 2017 a new human machine interface (HMI) for the control of upper limb prostheses, which is called the *myokinetic interface* [13]. Its mechanism is based on the transduction of the residual muscle physical movements/contractions into decipherable signals for the prosthetic hand. The HMI was originally conceived for trans-radial amputations, and foresees the implantation of small permanent magnets inside the residual muscles. An external device (called localizer) can be used to track the displacement of the magnets following contraction, and this information can be directly translated into highly selective control signals for the prosthesis. This approach features many advantages: magnets are passive components, thus no power supply is needed; many magnets can be implanted to control multiple degrees of freedom (DoFs) simultaneously (direct control); the control can be physiologically appropriate, i.e., the same muscles devoted to a specific function in the natural hand are targeted to receive the implant.

With the present work, we aimed at assessing the feasibility of applying the myokinetic interface to proximal amputations in TMR patients. The myokinetic approach appears particularly beneficial for TMR patients because, especially when the reinnervation targets the chest muscles, the latter undergo a conspicuous displacement during contraction, perceivable to the eye. This feature advocates the use of a HMI based on displacement, vice-versa it represents a considerable drawback for the use of sEMG electrodes which adhesion to the skin surface could be compromised [12]. This study did not involve the implantation of magnets, and was intended as a proof-of-concept of the approach. We sought to evaluate the possibility of disentangling the muscle movements by tracking their displacement from the surface, to discriminate different patterns associated with different DoFs of the missing limb.

Two participants with a proximal upper limb amputation, respectively at the glenohumeral and trans-humeral level, who underwent TMR surgery agreed to take part in this study. In a first experimental session, we verified the feasibility of using video analysis to detect the participant's intended action. In a second experimental session, we verified the feasibility of reaching the same goal by anchoring five small permanent magnets on the skin and tracking their displacement. The video analysis allowed to assess the approach using a simplified setup and an unlimited number of tracking points, thus acting as a baseline for the envisioned myokinetic system. Six different movements associated with three DoFs of the lost limb were performed by the participants, and a regularized logistic regression was used to discriminate the different movements. Our results show that it is possible to accurately classify unseen data and thus distinguish different movements, both from video recordings and with the myokinetic approach. These outcomes pave the way towards the translation of the myokinetic approach to TMR patients, taking advantage of the extensive movements of the reinnervated muscles to suggest a novel and usually unexploited control source for artificial hands.

II. MATERIALS AND METHODS

This study was approved by the Ethical Committee of the Medical University of Vienna (MUV) (EK Nr: 1393/2021). The

participants formally consented their participation in the study, as well as the publication of their recording sessions by signing the informed consent. The experimental sessions took place at the Clinical Laboratory for Bionic Extremity Reconstruction of the Medical University of Vienna, Austria. Two participants, referred to in the following as S1 and S2, were enrolled in this study. S1 is a 50-years-old man who suffered from a glenohumeral amputation, and S2 is a 32-years-old man who suffered from a trans-humeral amputation. Both amputations interested the left limb and had a traumatic origin, and the participants underwent TMR surgery at least six years prior to their participation in this study. In the former case, reinnervation mostly interested the muscles of the chest, while in the latter all the nerves were redirected to innervate muscles of the upper arm (Fig. 1). Both participants used myoelectric prostheses and were able to generate independent control signals for three DoFs corresponding to six movements, namely hand closing-opening (HC-HO), wrist supination-pronation (WS-WP, not implemented in the prosthesis of S2 due to weight constraints), and elbow flexion-extension (EF-EE) (see reinnervation matrices in Fig. 1). Data were processed offline using Matlab R2020b (The Mathworks, Natick, USA).

A. Vision Based Approach

The participants were asked to expose the skin over the reinnervated sites. Markers were drawn on the skin to allow the tracking of different body parts through video analysis. Patients were asked to contract the reinnervated muscles, and the marker sites were established following visual inspections of the skin, in order to maximize their displacement. Some markers were later added during offline analysis by exploiting anatomical landmarks (e.g., a scar) (Fig. 1). Two cameras were placed respectively in front and to the side of the participants, to simultaneously visualize all markers. Overall, 6 (10) and 7 (6) markers were selected for S1 (S2) in the frontal and lateral video, respectively. A Graphical User Interface (GUI) running on the laptop prompted and temporized through a progression bar the movements that the participants had to perform, among the three DoFs restored by the reinnervation (Fig. 2). Antagonist pair movements were always presented one after the other. Participants were asked to contract their muscles at 80% their maximum voluntary contraction (MVC). The GUI was realized as a custom C# application. The following datasets were acquired:

1) *Ordered Sequence (OS)*: Participants performed in sequence, for 10 consecutive times, the three antagonist pair movements (HC-HO, WS-WP, and EF-EE) (Fig. 2). They were asked to reach each target as fast as possible and to maintain the relative contraction for 5 s, with a 3s break within antagonist movements, and 5s break within consecutive pairs. Two repetitions were done, so that each movement was performed 20 times overall.

2) *Random Sequence (RS)*: The three antagonist pair movements were prompted by the GUI in a randomized order, using the same temporization of the OS dataset. The acquisition was stopped by the experimenter, after a minimum of nine and a maximum of 15 pair movements had been performed. The aim was to eliminate the bias caused by the fixed sequence, so that the

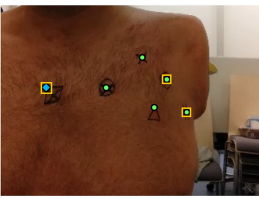
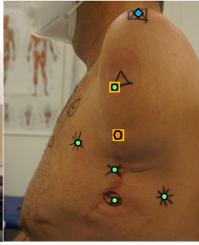
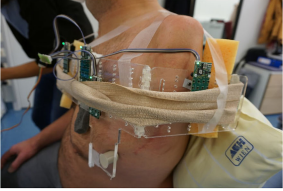


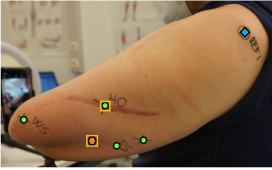
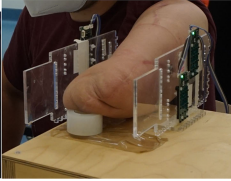
	Frontal camera	Lateral camera	Localizer setup	Targeted muscles	Nerves	Intended movement	
S1				Pectoral major clavicular part	Musculocutaneus	Elbow flexion	T
				Pectoral minor	Ulnar	Hand closing	T
				Pectoral major sternocostal part	Median Part I	Hand closing / wrist pronation	T
				Pectoral major abdominal part	Median Part II	Hand closing / wrist pronation	T
				Latissimus dorsi / Teres major	Radial	Elbow extension / wrist supination / hand opening	T
				Biceps long head	MC	Elbow flexion	O
S2				Biceps short head	Ulnar	Hand closing	T
				Brachialis	Median	Pronation	T
				Triceps long and medial head	Radial	Elbow extension	O
				Triceps lateral head	Split deep radial branch	Hand opening	T
				Brachioradialis	Split deep radial branch	Supination	T

Fig. 1. Placement of markers (left) and permanent magnets (middle) over the reinnervated sites for both S1 (up) and S2 (down), and setup used for localizing the magnets (right). The reinnervation matrix of both S1 and S2 is also reported (T stand for “Transferred”, while O stands for “Original”).

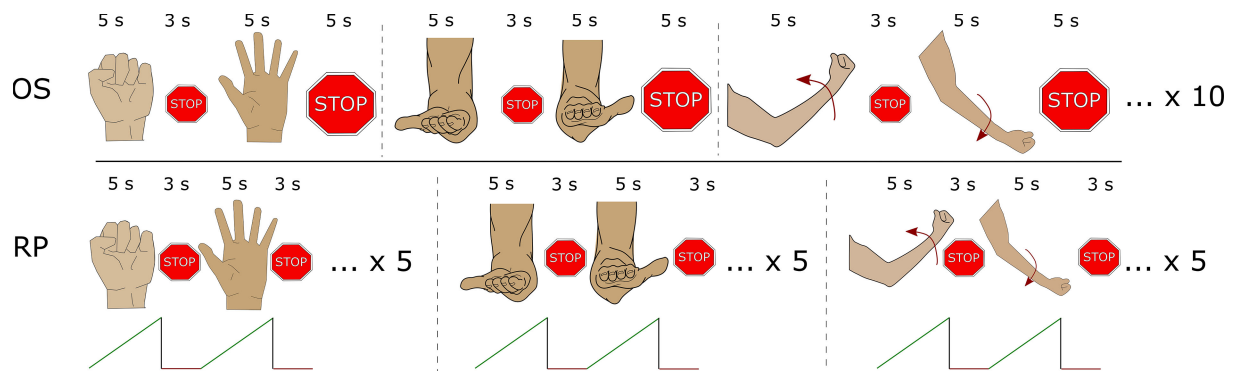


Fig. 2. Commands shown and timings prompted by the GUI for the acquisition of dataset OS (up) and RP (down).

participant was not aware of the following/upcoming requested movement.

3) *Repeated Pairs (RP)*: Each antagonist pair movement was repeated consecutively for five times. Unlike OS and RS datasets, in which the 80% MVC was to be reached as fast as possible, here the GUI showed a saw-tooth signal increasing from 0 to 5 in equal steps in the 5s interval of each movement (Fig. 2). The participant was asked to incrementally contract the muscles (up to 80% MVC), following the increasing signal. The aim was to assess the performance of the classifier when the final posture was reached gradually.

Frontal and lateral videos were recorded at 30 fps and were synchronized by means of an acoustic signal generated by the GUI at the beginning of each acquisition. The 2D coordinates of each marker were extracted using the DeepLabCut Python library [14]. As a result, two time series were derived from each marker. The 2D coordinates of one reference marker per video (the less moving one, Fig. 1) was subtracted from the remaining ones, and detrending was applied to the obtained time series.

A sliding window of 300ms (named feature window length, FWL) with a 200 ms step was then applied, corresponding to five steps per second (4% the movement duration each). For each window, nine features were extracted, specifically: maximum value, minimum value, range (maximum-minimum), mean value, standard deviation, mean time-differential and mean time-differential sign, root-mean-square value, and median value. In addition, the mean value and the mean time-differential sign of the distance between consecutive (i.e., near) markers and of the angle between two vectors identified by three consecutive markers were also extracted. Given the slight different amount of markers, this resulted in a total of 242 and 308 features for S1 and S2, respectively.

B. Myokinetic Approach

Five cylindrical magnets (2×4 mm) were anchored to the participants' skin (number of magnets limited by setup constraints). The placement of the magnets was guided by the

position of the markers employed for video analysis which had shown larger displacements (Fig. 1). The acquisitions made in the first session (i.e., OS, RS, and RP) were repeated. An external magnetic acquisition system, consisting of four boards mounting 20 3-axial magnetic field sensors each (LIS3MDL, STMicroelectronics, Switzerland), was used to acquire the magnetic field generated by the magnets. A custom plexiglass frame and elastic straps were used to hold the acquisition boards in place (Fig. 1). The acquisition system was connected to a computation unit (Computer-on-Module board iMXRT1062 OEM, Embedded Artists, Sweden). A localization algorithm, already developed and assessed in previous studies [13], [15], [16], was implemented on the computation unit and used to continuously localize the pose of the magnets (i.e., position and orientation in space) online. The retrieved poses were thus sent to the laptop (serial communication), and saved for offline analysis. The acquisition of the sensors was triggered by the C# application, so that the acquired data were automatically synchronized with the participant's movements.

The poses of the magnets was used to derive time series of the: relative displacement (i.e., Euclidean distance) of each magnet from its initial position; relative displacement between all possible couples of magnets; difference of the x, y, z coordinates from their initial values for each magnet; difference of the x, y, z coordinates between all possible couples of magnets; angular displacement between all possible couples of magnets. The computation unit provided an updated magnets' pose 32 times per second. A FWL of 375ms, with a 250ms step was applied, corresponding to four steps per second (5% the movement duration each). For each time series the same nine features used for the video data were extracted, resulting in a total of 630 features.

C. Classification Algorithm

For both approaches (video and myokinetic) the features extracted from the two OS acquisitions were concatenated for training. In particular, among the 20 repetitions, 17 (85%) were randomly selected. A one vs. all approach was applied, thus six logistic regressors were trained to recognize each of the six movements. The response vectors were binary encoded by setting the label to one for the 5s duration of the target movement, and to zero otherwise. Then, a feature selection strategy was implemented. First, for each class (i.e., each movement) a subset of features was selected based on the correlation coefficient (ρ) between the class and the feature (a cut-off threshold was used to exclude features below such threshold). Then, a further selection was implemented by applying Principal Components Analysis (PCA) and retaining only the principal components that explained a certain percentage amount (called *exp*) of data variation. Both the value of ρ and *exp* were experimentally set for each class based on the performance of the regressor on the development set. A coefficient representative of the relevance of each feature was computed. First, the number of times a feature was selected based on ρ was derived; then, the obtained values were multiplied for the sum of the loadings of each feature in the

TABLE I
PARAMETERS USED FOR FEATURE SELECTION, NUMBER OF SELECTED PRINCIPAL COMPONENTS (PC) AND FEATURE REDUCTION PERCENTAGE BASED ON ρ (%), AND LOGISTIC REGRESSOR HYPERPARAMETER LAMBDA

	HC	HO	WS	WP	EF	EE
ρ	0.1 ^a	0.1	0.1	0.1	0.1	0.1
	0.01 ^b	0.01	0.01	0.01	0.01	0.01
	0.01 ^c	0.01	0.01	0.01	0.01	0.01
	0.01 ^d	0.01	0.01	0.01	0.01	0.01
<i>exp</i>	99.9	99.9	99.9	99.9	99.9	99.9
	99	99	99	99	99	99
	90	99	99	99	95	95
	90	90	90	90	99	99
#PC (%)	47 (61)	51 (66)	45 (66)	62 (49)	63 (49)	56 (58)
	80 (29)	90 (23)	86 (25)	89 (21)	72 (31)	86 (30)
	20 (39)	81 (47)	85 (41)	115 (15)	42 (30)	44 (33)
	30 (38)	32 (41)	28 (43)	41 (27)	108 (36)	104 (53)
Lambda	0.014	0.0015	6*10 ⁻⁴	0.0013	7*10 ⁻⁵	0.0024
	0.0015	0.0012	0.0010	0.0011	0.0011	0.0013
	0.0015	0.0026	0.0037	0.0048	0.0014	0.0011
	2*10 ⁻⁵	0.0027	0.0017	8*10 ⁻⁴	0.0011	0.0019

^aS1-v. ^bS2-v. ^cS1-m. ^dS2-m.

selected PCA eigenvectors. Results were normalized, resulting in coefficients in the [0,1] range. The model was internally validated following a 10-fold cross-validation approach using the Matlab function *lassoglm* with default parameters. This function implements a regularized logistic regression with a lasso penalty, using a geometric sequence of Lambda values. The value of Lambda corresponding to the minimum cross-validation error was finally selected (Table I). In addition, to limit the effect of class unbalance, we weighted the cost of less represented samples during training by a fixed factor of 10. A thresholding operation (threshold = 0.6) was applied to the regressor output to get the final binary classification. If multiple logistic regressors returned a probability estimate higher than 60% in the same time window, the one having the highest probability was selected as winner. The threshold allowed to reject uncertain classifications and to identify windows not relative to a motor intention (i.e., time intervals between classes), indicated in the following as rest.

D. Performance Metrics

The F1-score was used to evaluate the trained model, as it gives a more thorough representation of the classifier performance compared to accuracy in case of unbalanced classes. The F1-score is defined in the following way:

$$F1 - score = \frac{2TP}{2TP + FP + FN}$$

where TP are the true positives, FP the false positives, and FN the false negatives. Also in this case, a one-vs-all approach was applied to compute the F1-score for each class. The model was tested on three different datasets, namely the three repetitions of OS (15%) left out from the training set (in the following called Test), the RS dataset, and the RP dataset.

III. RESULTS

In the following, we will refer to S1-v (S2-v) and S1-m (S2-m) for indicating the data acquired during the vision and myokinetic

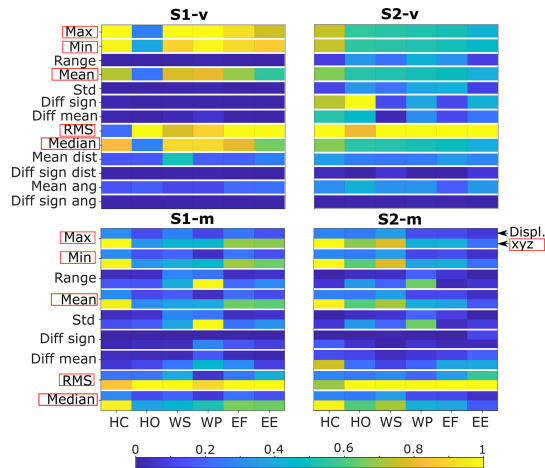


Fig. 3. Feature selection results. Features were grouped across markers/magnets. In the magnetic case (below), a distinction was made between those derived from Euclidian and angular distances (Displ.) and independent cartesian coordinates (x, y, z). The colorbar encodes the coefficient (in [0, 1]) representing the relevance of each feature. Features showing higher coefficients are indicated by the red boxes. Legend: HC-Hand Closing, HO-Hand Opening, WS-Wrist Supination, WP-Wrist Pronation, EE-Elbow Extension, EF-Elbow Flexion.

experimental session with S1 (S2), respectively. Table I reports the ρ and exp values, the number of selected Principal Components and the percentage of feature reduction following the ρ thresholding, as well as the selected Lambda value used for training the logistic regression models. The obtained coefficients showed a clear pattern across classes and data types, as five features (namely Min, Max, Mean, RMS and Median) generally showed higher coefficients than the remaining ones (Fig. 3). Notably, for the magnetic data, features derived from the xyz coordinates proved more informative than those obtained from relative distances. Considering first a representative result, i.e., the RS dataset from S1-v, the classifier proved accurate in discriminating the different movements, showing a minimum F1-score of 0.69 for class WS, and a maximum F1-score of 0.89 for both HO and EE class (Fig. 4 and Supplementary Video). More in general, in the majority of mis-classification cases movements were recognized as rest state or vice-versa, while few times they were exchanged across each other (Fig. 4(b)). This is in line with the visual evidence that the pattern of displacement of the markers (Fig. 4(a)) appears clearly distinguishable, as well as repeatable in correspondence of the different movements. Not surprisingly, most of the times mis-classifications occurred in the transient phase between movements and rest (Fig. 4(a)). This appeared more evident in the early portion of the ramp of dataset RP, S1-v (Fig. 5). Indeed, the confidence of the regressors in recognizing the corresponding class showed a monotonic increase (Spearman coefficient = 0.99, $p < .01$), and the same held true for the RP datasets of S1-m, S2-v and S2-m (not shown).

Overall, the classifier showed good performance for all classes, even if appreciably higher F1-scores were obtained for S1 compared to S2 (i.e., for the more proximal amputation level, Table II–Fig. 6). Moreover, for both S1 and S2 the performance proved generally better when considering video

TABLE II
F1-SCORES FOR VIDEO AND MAGNETIC DATA, FOR BOTH PARTICIPANTS AND ALL CLASSES

	Dataset	F1-score					
		HC	HO	WS	WP	EF	EE
S1-v ^a	Test	0.92	0.83	0.85	0.90	0.90	0.88
	RS	0.84	0.89	0.69	0.83	0.87	0.89
	RP	0.84	0.69	0.84	0.88	0.87	0.77
S1-m ^b	Test	0.88	0.77	0.83	0.66	0.87	0.80
	RS	0.90	0.68	0.73	0.57	0.63	0.84
	RP	0.55	0.31	0.60	0.42	0.77	0.59
S2-v	Test	0.67	0.63	0.78	0.88	0.69	0.54
	RS	0.60	0.51	0.79	0.81	0.58	0.68
	RP	0.22	0.49	0.83	0.80	0.57	0.60
S2-m	Test	0.65	0.83	0.81	0.81	0.75	0.62
	RS	0.52	0.82	0.65	0.78	0.56	0.64
	RP	0.24	0.64	0.62	0.24	0.20	0.45

^aVideo data. ^bMyokinetic approach.

data in comparison to the myokinetic approach, even if such difference proved statistically significant only for datasets Test and RP of S1 (Mann-Whitney U Test, Fig. 6). Overall, the average F1-score computed across all test datasets decreased by a maximum of 0.32 (0.22) for class WP (WP) relative to S1 (S2). Nevertheless, the accuracy trend across different classes was generally maintained for both approaches (video and magnetic) and participants. Indeed, for both S1-v and S1-m, the classifiers proved always robust in detecting HC and EF, with an average F1-score of 0.87 and 0.88 in the former case, and of 0.78 and 0.76 in the latter. Considering S2-v and S2-m, the same generally held true for class WS, with an average F1-score of 0.80 in the former case, and of 0.69 in the latter. A performance deterioration was observed for some classes when testing the classifier on the RP datasets, with a particular F1-score drop for class EF in S2-m (F1-score = 0.20) (Table II). In this case, $\sim 48\%$ of the windows belonging to class EF were wrongly classified as class HC (not shown).

As expected, the average F1-score computed across classes proved always higher when the model was evaluated on the Test dataset (Fig. 6). Indeed, the same trend was maintained across all conditions (i.e., S1-v, S1-m, S2-v, and S2-m), showing the lowest average F1-scores obtained always for the RP datasets. Overall, the average F1-scores computed on each dataset proved always above the random guess line (~ 0.17) (Fig. 6).

IV. DISCUSSION

In this study, we assessed for the first time the feasibility of applying the myokinetic approach to TMR patients. Our outcomes answer the following research questions: can we disentangle different muscle movements, associated with different postures, by analysing videos of the participant performing such postures? Can we place some permanent magnets on the skin and track their displacement, to control multiple DoFs of an artificial hand? Using video analysis and the myokinetic interface to monitor the skin displacement over the reinnervated sites of two participants, we proved the viability of disentangling different

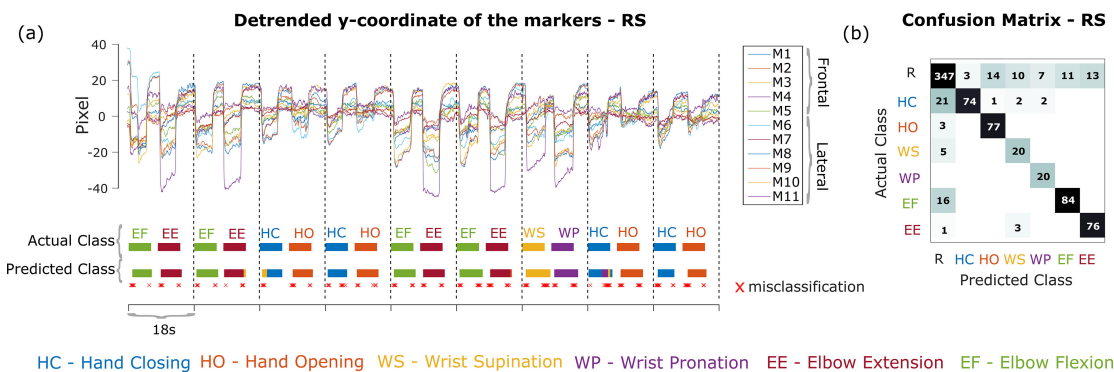


Fig. 4. Representative classification output relative to the RS dataset for S1 and video data (S1-v). (a) Raw displacement of the y-coordinates of all markers (M1–M11) following subtraction of the reference marker and detrending, classification output for the prompted pair movements, and misclassification errors (red crosses). (b) Confusion matrix.

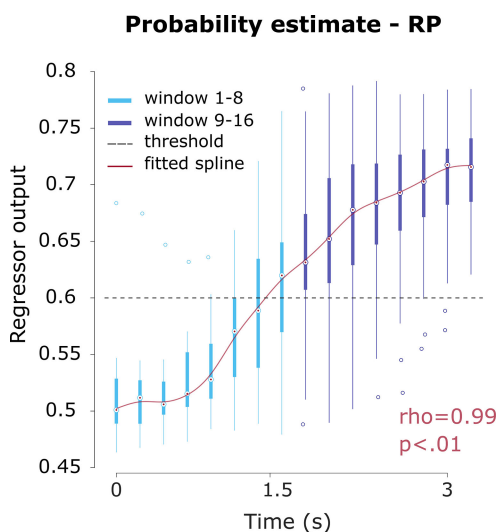


Fig. 5. Early ramp portion, dataset RP of S1-v. Boxplots (including data in the interquartile range) represent the logistic regressors output grouped across classes and repetitions. In the first ~3s of the ramp, a monotonic increase in the confidence of the regressors in recognizing the corresponding class is found (Spearman coefficient (ρ) of 0.99 and $p < .01$ for the spline fitted on the boxplot medians).

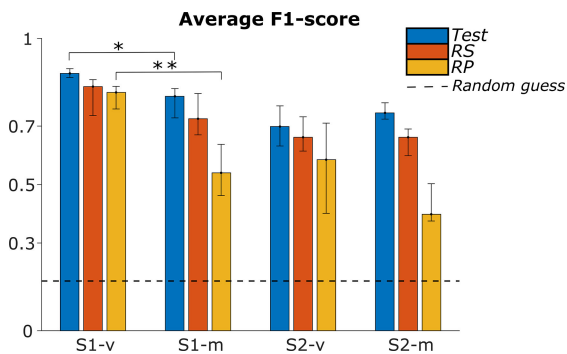


Fig. 6. Average F1-score for the three test datasets (Test, RS, and RP), grouped for each participant (S1 and S2), derived from videos (S1-v, S2-v) and with the myokinetic approach (S1-m, S2-m). The dashed line represents the random guess line. When comparing the outcomes from magnetic and video data, the latter showed significantly higher F1-scores for datasets Test and RP of S1 ($p < .05$ and $p < .01$, respectively).

patterns of movement to accurately discriminate six movements of the lost limb.

As expected, lower F1-scores were generally achieved for S2 compared to S1, for both experimental sessions (Table II, Fig. 6). We impute this lower classification score to anatomical factors: first, the skin displacement induced by muscle contraction was significantly smaller in S2, due to different anatomical conditions (arm vs chest muscles). Secondly, while for S1 an extensive skin surface covering the reinnervation sites was available, for S2 all the acquisitions were made from the narrower surface of the stump. This plausibly led to more important cross-talk effects among different movements, making it more challenging to disentangle them from the surface.

Since a binary encoding (on-off activation) of the different movements was applied, it appears plausible that most misclassifications occurred in the transient phase across rest and movement windows (Fig. 4(a)). This likely explains also the (sometimes significant) drop in accuracy obtained when testing the trained models on the RP datasets, as demonstrated by the monotonic trend in the logistic regressor output found in the early portion of the ramp (Fig. 5). Indeed, reaching the final posture gradually is equivalent to extending the transient phase. Notably, the drop in accuracy for RP involved movements somehow functionally coupled. For instance, HC and EF in S2 are both operated by the biceps (Fig. 1), thus their activation likely generates similar displacements when monitoring the skin surface. This was less evident for S1, possibly because of the clearer distinction among reinnervated areas. The lower F1-score obtained for HO in RP of S1-m (0.31) can probably be ascribed to setup constraints. Indeed, HO was restored by redirecting the radial nerve to innervate muscles of the lateral side (Fig. 1), which movement could only be partially recorded with the myokinetic interface. Finally, it is worth considering that, despite the precise temporization of the GUI and the accurate class encoding, a delay in the actual initiation/conclusion of the movement by the participant was sometimes present (see Supplementary Video).

The present study was limited in some respects. First, only elementary movements were investigated, however the feasibility of using combined outputs from the regressors should

be assessed in future implementations. Nevertheless, we are currently unable to establish whether the training patterns used here would be significantly altered by combined DoFs. Regarding the myokinetic approach, the performance could reasonably be improved by designing custom sockets for each participant to hold the acquisition boards, in order to optimize the sensor placement and to avoid possible mechanical disturbances which alter the sensor measurements among different acquisitions. Moreover, since the movement generated by different muscles on the skin is not completely independent due to anatomical factors, like the presence of connective tissue (especially considering different compartments of the same muscle, e.g., the biceps), more distinguishable signals could be obtained by implanting the magnets inside the muscles. However, this study being a proof-of-concept, the achieved outcomes showed good performance, keeping in mind the limitations imposed by the anatomical factors.

The outcomes of this work encourage further studies on a novel control strategy for TMR patients, based on the transduction of movements in place of electrical signals. They pave the way towards the investigation of a poorly explored field, which nonetheless appears to bring many advantages for the restoration of the lost functionalities.

ACKNOWLEDGMENT

The authors would like to thank S1 and S2 for taking part in this study and for supporting their research.

REFERENCES

- [1] F. Cordella *et al.*, "Literature review on needs of upper limb prosthesis users," *Front. Neurosci.*, vol. 10, pp. 1–14, 2016, doi: [10.3389/fnins.2016.00209](https://doi.org/10.3389/fnins.2016.00209).
- [2] O. C. Aszmann and D. Farina, *Bionic Limb Reconstruction*. Berlin/Heidelberg, Germany: Springer, 2021.
- [3] K. Ziegler-graham *et al.*, "Estimating the prevalence of limb loss in the United States: 2005 to 2050," *Arch. Phys. Med. Rehabil.*, vol. 89, pp. 422–429, 2008, doi: [10.1016/j.apmr.2007.11.005](https://doi.org/10.1016/j.apmr.2007.11.005).
- [4] P. F. Pasquina *et al.*, "First-in-man demonstration of a fully implanted myoelectric sensors system to control an advanced electromechanical prosthetic hand," *J. Neurosci. Methods*, vol. 244, pp. 85–93, 2015, doi: [10.1016/j.jneumeth.2014.07.016](https://doi.org/10.1016/j.jneumeth.2014.07.016).
- [5] T. A. Kuiken, G. A. Dumanian, R. D. Lipschutz, L. A. Miller, and K. A. Stubblefield, "The use of targeted muscle reinnervation for improved myoelectric prosthesis control in a bilateral shoulder disarticulation amputee," *Prosthetics Orthotics Int.*, vol. 28, pp. 245–253, 2004, doi: [10.3109/03093640409167756](https://doi.org/10.3109/03093640409167756).
- [6] E. Mastinu, P. Doguet, Y. Botquin, B. Hakansson, and M. Ortiz-Catalan, "Embedded system for prosthetic control using implanted neuromuscular interfaces accessed via an osseointegrated implant," *IEEE Trans. Biomed. Circuits Syst.*, vol. 11, no. 4, pp. 867–877, Aug. 2017, doi: [10.1109/TB-CAS.2017.2694710](https://doi.org/10.1109/TB-CAS.2017.2694710).
- [7] M. Controzzi, F. Clemente, D. Barone, A. Ghionzoli, and C. Cipriani, "The SSSA-MyHand: A dexterous lightweight myoelectric hand prosthesis," *IEEE Trans. Neural Syst. Rehabil. Eng.*, vol. 25, no. 5, pp. 459–468, May 2017, doi: [10.1109/TNSRE.2016.2578980](https://doi.org/10.1109/TNSRE.2016.2578980).
- [8] M. Laffranchi *et al.*, "The Hannes hand prosthesis replicates the key biological properties of the human hand," *Sci. Robot.*, vol. 5, no. 46, 2020, Art. no. eabb0467, doi: [10.1126/SCIROBOTICS.ABB0467](https://doi.org/10.1126/SCIROBOTICS.ABB0467).
- [9] M. Ortiz-Catalan, B. Håkansson, and R. Brånemark, "An osseointegrated human-machine gateway for long-term sensory feedback and motor control of artificial limbs," *Sci. Transl. Med.*, vol. 6, no. 257, 2014, Art. no. 257re6, doi: [10.1126/scitranslmed.3008933](https://doi.org/10.1126/scitranslmed.3008933).
- [10] D. Farina *et al.*, "Toward higher-performance bionic limbs for wider clinical use," *Nature Biomed. Eng.*, pp. 1–13, 2021, doi: [10.1038/s41551-021-00732-x](https://doi.org/10.1038/s41551-021-00732-x).
- [11] S. Salminger *et al.*, "Long-term implant of intramuscular sensors and nerve transfers for wireless control of robotic arms in above-elbow amputees," *Sci. Robot.*, vol. 4, no. 32, 2019, Art. no. eaaw6306, doi: [10.1126/scirobotics.aaw6306](https://doi.org/10.1126/scirobotics.aaw6306).
- [12] C. J. De Luca, L. D. Gilmore, M. Kuznetsov, and S. H. Roy, "Filtering the surface EMG signal: Movement artifact and baseline noise contamination," *J. Biomech.*, vol. 43, no. 8, pp. 1573–1579, 2010, doi: [10.1016/j.jbiomech.2010.01.027](https://doi.org/10.1016/j.jbiomech.2010.01.027).
- [13] S. Tarantino, F. Clemente, D. Barone, M. Controzzi, and C. Cipriani, "The myokinetic control interface: Tracking implanted magnets as a means for prosthetic control," *Sci. Rep.*, vol. 7, no. 1, 2017, Art. no. 17149, doi: [10.1038/s41598-017-17464-1](https://doi.org/10.1038/s41598-017-17464-1).
- [14] A. Mathis *et al.*, "DeepLabCut: Markerless pose estimation of user-defined body parts with deep learning," *Nature Neurosci.*, vol. 21, pp. 1281–1289, 2018, doi: [10.1038/s41593-018-0209-y](https://doi.org/10.1038/s41593-018-0209-y).
- [15] F. Clemente, V. Ianniciello, M. Gherardini, and C. Cipriani, "Development of an embedded myokinetic prosthetic hand controller," *Sensors*, vol. 19, 2019, Art. no. 3137, doi: [10.3390/s19143137](https://doi.org/10.3390/s19143137).
- [16] M. Gherardini, F. Clemente, S. Milici, and C. Cipriani, "Localization accuracy of multiple magnets in a myokinetic control interface," *Sci. Rep.*, vol. 11, no. 1, pp. 1–10, 2021, doi: [10.1038/s41598-021-84390-8](https://doi.org/10.1038/s41598-021-84390-8).